MNRAS 000, 1–12 (2020) Preprint 5 February 2020 Compiled using MNRAS LATEX style file v3.0

The ALPINE–ALMA [CII] Survey: On the nature of an extremely obscured serendipitous galaxy

M. Romano[⋆1,2], P. Cassata[1,2], L. Morselli[1,2], B. C. Lemaux[3], M. Béthermin[4], P. Capak[5,6,7], A. Faisst[5], O. Le Fèvre[4], D. Schaerer[8,9], J. Silverman[10,11], L. Yan[12], S. Bardelli[13], M. Boquien[14], A. Cimatti[15,16], M. Dessauges-Zavadsky[8], A. Enia[1,2], Y. Fudamoto[8], S. Fujimoto[6,17], M. Ginolfi[8], C. Gruppioni[13], N. P. Hathi[18], E. Ibar[19], G. C. Jones[20,21], A. M. Koekemoer[18], F. Loiacono[13,15], C. Mancini[1], D. A. Riechers[22,23], G. Rodighiero[1,2], L. Rodríguez-Muñoz[1], M. Talia[13,15], L. Vallini[24], D. Vergani[13], G. Zamorani[13], and E. Zucca[13]

(Affiliations are listed at the end of the paper)

arXiv:2002.00961v1 [astro-ph.GA] 3 Feb 2020

Accepted XXX. Received YYY; in original form ZZZ

ABSTRACT

We report the serendipitous discovery of a bright galaxy (Gal-A) observed as part of the ALMA Large Program to INvestigate [CII] at Early times (ALPINE). While this galaxy is detected both in line and continuum emission in ALMA Band 7, it is completely dark in UV/optical filters and only presents a marginal detection in the UltraVISTA K_s band. We discuss the nature of the observed ALMA line, i.e. whether the emission comes from [CII] at $z \sim 4.6$, or from high-J CO transitions at $z \sim 2.2$. In the first case we find a [CII]-to-FIR luminosity ratio of $\log(L_{[CII]}/L_{FIR}) \sim -2.5$, consistent with the average value for local star-forming galaxies (SFGs); in the second case, instead, the source would lie outside of the empirical relations between L_{CO} and L_{FIR} found in the literature. At both redshifts, we derive the star-formation rate (SFR) from the ALMA continuum, and the stellar mass (M_*) by using stellar population synthesis models as input for LePHARE spectral energy distribution (SED) fitting. Exploiting our results, we believe that Gal-A is a "Main-Sequence" (MS), dusty SFG at $z = 4.6$ (i.e. [CII] emitter) with $\log(SFR/[M_\odot yr^{-1}]) \sim 1.4$ and $\log(M_*/M_\odot) \sim 9.7$. This work underlines the crucial role of the ALPINE survey in making a census of this class of objects, in order to unveil their contribution to the global star-formation rate density (SFRD) of the Universe at the end of the Reionisation epoch.

Key words: galaxies: evolution – galaxies: high-redshift

1 INTRODUCTION

The last decades have seen dramatic advances in our knowledge of galaxy formation and evolution (Giavalisco 2002; Renzini 2006; Silk & Mamon 2012; Carilli & Walter 2013; Madau & Dickinson 2014; Naab et al. 2017). The global star-formation rate density (SFRD) has been found to rise during cosmic reionisation from $z \sim 10$, peak at $1 < z < 3$, and finally decrease by a factor of ~ 10 to the local Universe (Lilly et al. 1996; Bouwens et al. 2011; Madau & Dickinson 2014). Several studies suggest that, at all epochs, the bulk of the star-formation activity takes place in galaxies lying on the "Main-Sequence" (MS): a tight correlation between the star-formation rate (SFR) and the stellar mass (M_*; Daddi et al. 2007; Rodighiero et al. 2011; Speagle et al. 2014; Santini et al. 2017). Therefore, we have indications that most of the stars in the Universe formed along the MS, at the peak of the SFRD at $z \sim 2$. However, we are still trying to understand which are the main mechanisms responsible for the rapid increase of the SFRD at $z < 6$. One possible explanation is an increase in the gas fraction along with a rising in star-formation efficiency per unit mass, possibly driven by galaxy mergers (Genzel et al. 2015; Silverman et al. 2015; Scoville et al. 2016).

⋆ E-mail: michael.romano@studenti.unipd.it

© 2020 The Authors

At $z > 3$ the cosmic SFRD is almost exclusively constrained by UV-selected samples (Bouwens et al. 2012a,b; Schenker et al. 2013; Oesch et al. 2015), lacking information about the star formation obscured by dust. Rest-frame UV-selected galaxies must be corrected for dust absorption: wrong dust corrections can lead to large uncertainties on the SFR estimates and, consequently, to an incorrect picture of the star-formation history (SFH) of the Universe (Gallerani et al. 2010; Castellano et al. 2014; Scoville et al. 2015; Álvarez-Márquez et al. 2016). At the same time, heavily dust-obscured star-forming galaxies (SFGs) may be completely missed by surveys probing rest-frame UV/optical emission.

With the advent of new facilities, such as the Atacama Large Millimiter Array (ALMA), a population of faint, dusty SFGs has been confirmed at high redshift, e.g. sub-millimiter galaxies (Dunlop et al. 2004; Daddi et al. 2009; Riechers et al. 2010; Huang et al. 2014; Santini et al. 2016), ALMA-only sources (e.g. Williams et al. 2019), the extremely red objects selected with H and IRAC colors (HIEROs galaxies) from Wang et al. (2016). While the bulk of these objects peaks at $2 < z < 3$, a significant tail of higher redshift, dusty galaxies without optical/near-infrared (NIR) detections is in place at $z > 4$ (Capak et al. 2008; Daddi et al. 2009; Riechers et al. 2010; Walter et al. 2012; Riechers et al. 2013; Pavesi et al. 2018). For instance, Walter et al. (2012) combined measurements from the IRAM Plateau de Bure Interferometer (PdBI) and the Jansky Very Large Array (VLA) to put constraints on the dust-obscured starburst HDF850.1, one of the first detected optical/NIR invisible galaxies. This source is at $z = 5.18$ among an overdensity of galaxies at the same redshift, with a [CII]/FIR luminosity ratio comparable to that observed in local SFGs. In addition, most of these objects are often extreme starbursts, such as HFLS3. This source is confirmed to be at $z = 6.34$ exploiting information from different molecular and atomic fine structure cooling lines and shows a large FIR luminosity (i.e. $L_{FIR} \sim 2 \times 10^{13}$ $L_\odot$) and SFR $> 10^3$ $M_\odot$/yr (Riechers et al. 2013).

An in-depth study of this elusive population of galaxies is necessary in order to complete the census of SFGs at high redshift contributing to the cosmic SFH as well as to better understand the early phases of the galaxy formation (Blain et al. 2002; Casey et al. 2014).

In this context, the ALMA Large Program to INvestigate [CII] at Early times (ALPINE; Béthermin et al. in prep.; Faisst et al. 2019; Le Fèvre et al. 2019) is going to improve our knowledge of the obscured star formation at $z > 4$. It takes advantage of observations of the singly ionised carbon [CII] at 158 μm and its adjacent FIR continuum for a sample of 118 SFGs in the Cosmic Evolution Survey (COSMOS; Scoville et al. 2007a,b) and the Extended Chandra Deep Field South (E-CDFS; Giavalisco et al. 2004; Cardamone et al. 2010) fields. These sources are spectroscopically confirmed to be at $4 < z < 6$ with the Visible Multi-Object Spectrograph (VIMOS) at the Very Large Telescope (VLT; Le Fèvre et al. 2003, 2015) and with the DEep Imaging Multi-Object Spectrograph (DEIMOS) at the Keck II telescope (Faber et al. 2003; Hasinger et al. 2018).

The [CII] line is one of the strongest lines in the FIR band (e.g. Stacey et al. 1991) as it is one of the main coolants of the interstellar medium (ISM; Carilli & Walter 2013). Since it has a lower ionisation potential than neutral hydrogen (HI), i.e. 11.3 eV compared to 13.6 eV, this line can trace different gas phases, such as dense photodissociation regions (PDRs; Hollenbach & Tielens 1999), neutral diffuse gas (e.g. Wolfire et al. 2003; Vallini et al. 2015), and diffuse ionised gas (e.g. Cormier et al. 2012). In principle, in order to remove the ambiguity on the interpretation of the [CII] emission, the relative contribution of the various gas phases should be assessed. However, different studies suggest that the bulk of the [CII] emission arises from the external layers of molecular clouds heated by UV photons in PDRs (Stacey et al. 1991; Madden et al. 1997; Kaufman et al. 1999; Cormier et al. 2015; Pavesi et al. 2016); thus, this line can be used as a tracer of star formation (e.g. De Looze et al. 2014; but see also Zanella et al. 2018 who suggest that [CII] is a better tracer of the molecular gas). Therefore, the combination of FIR continuum and UV measurements, together with the [CII] observations, will provide, at the redshift explored by the ALPINE survey, an estimate of the total (obscured and unobscured) star formation in these galaxies, corresponding to 80-95% of the cosmic SFRD at $4 < z < 6$ (Casey et al. 2012; Bouwens et al. 2016; Capak et al. 2015; Aravena et al. 2016; Novak et al. 2017). The remaining 5-20% of star formation which is not traced by UV data is yielded by a free blind survey covering an additional area of 25 arcmin^2 beyond the targeted sources, where many galaxies have been serendipitously detected so far (Loiacono et al. in prep.). Among these, several sources are invisible in the optical bands. The study of these objects is crucial for obtaining a robust estimate of the total SFRD at $z > 4$ and for characterising the overall population of the high-redshift SFGs.

In this work, we discuss the nature of a galaxy (hereafter, Gal-A) randomly discovered in the field of the ALPINE target DEIMOS_COSMOS_665626 (hereafter, DC_665626). The galaxy has a spatial offset of ~ 6 arcsec (1 arcsec is ~ 7 kpc at $z = 4.583$, the redshift of the target) from DC_665626; it does not show any optical counterpart at the position of the emission detected with ALMA and, for this reason, its nature results to be ambiguous. Besides, since Gal-A is the brightest galaxy detected in line emission among all those having no optical counterpart and serendipitously observed in ALPINE so far (Loiacono et al. in prep.), this work can be exploited as a benchmark for future analysis on these types of sources.

The paper is organised as follows: in Section 2 we introduce the available data we have for Gal-A, and explain the methods used to analyse this source. We present the results in Section 3 and discuss them in Section 4, trying to constrain the nature of the galaxy. Summary and conclusions are provided in Section 5.

Throughout this paper, we assume a ΛCDM cosmology with $H_0 = 70$ km/s/Mpc, $\Omega_m = 0.3$, and $\Omega_\Lambda = 0.7$ (Planck Collaboration 2018). We furthermore use a Chabrier (2003) initial mass function (IMF) and AB magnitudes.

2 OBSERVATIONS AND DATA REDUCTION

2.1 ALMA data

DC_665626 has been observed with ALMA in Band 7 (ν_{obs} = [275 – 373] GHz) on 25 May 2018 (Cycle 5; Project 2017.1.00428.L, PI O. Le Fèvre) using 45 antennas with the

C43-2 array configuration (with a maximum baseline of ∼ 250 m). The on-source integration time is 16 minutes, with a total elapsed time of 37 minutes.

The spectral setup consists of two sidebands with a frequency range of $\Delta^{\rm l}_{\nu} \simeq [339 - 343]$ GHz and $\Delta^{\rm u}_{\nu} \simeq [351 - 355]$ GHz for the lower and upper sidebands, respectively. Each sideband is made up of two spectral windows (SPWs) of width 1.875 GHz, each of which containing 128 channels 15.625 MHz wide (the sidebands overlap for 7 channels), with a typical rms of 0.6 mJy beam^{-1} per channel. The flux and phase are calibrated using the standard calibrators J1058+0133 and J0948+0022, respectively.

The data are analysed using standard pipelines for ALMA reduction included in the software CASA (McMullin et al. 2007), version 5.4.0. The imaging is obtained running the `TCLEAN` task on the visibilities, setting a threshold of $3\sigma_{\rm rms}$ on the noise level when cleaning the data (where $\sigma_{\rm rms}$ is obtained from the dirty image), and with a natural weighting scheme to increase the sensitivity.

2.2 Identification of the serendipitous source

As part of the COSMOS field (Scoville et al. 2007a,b), which is one of the most thoroughly studied regions of the sky so far, multi-wavelength data are available for the whole ALPINE sample, including high-resolution Hubble Space Telescope (HST) imaging (Koekemoer et al. 2007, 2011), and photometry from the Canada-France-Hawaii Telescope (CFHT), the Spitzer telescope and other facilities (Capak et al. 2007; Laigle et al. 2016). Spectroscopic redshifts are available from large optical spectroscopic campaigns at the VLT (VUDS; Le Fèvre et al. 2015) and Keck (DEIMOS; Hasinger et al. 2018). Multi-band photometry and spectroscopic data allow to build spectral energy distributions (SEDs) and to derive robust parameters including SFRs and stellar masses through SED-fitting (Faisst et al. 2019). Through this analysis, we find that DC_665626 has $\log(M_*/M_\odot) = 9.21^{+0.16}_{-0.18}$, $\log(\mathrm{SFR}/[M_\odot \mathrm{yr}^{-1}]) = 0.71^{+0.29}_{-0.18}$, and a spectroscopic redshift of $z_{\rm spec} = 4.583$, obtained from Lyα emission and ISM absorption lines in the observed-frame optical spectrum.

Since the ALPINE target DC_665626 is at $z_{\rm spec} = 4.583$, the [CII] emission from this source ($\nu_{\rm rest} = 1900.54$ GHz) is expected to be redshifted at around $\nu_{\rm obs} = 340.42$ GHz, falling inside the lower sideband of the observed ALMA spectrum. When we inspect the cube, together with the [CII] emission coming from DC_665626 (at 4.4σ; Béthermin et al. in prep.), we identify a more significant emission with a spatial offset of ∼ 6" (∼ 40 proper kpc at $z \sim 4.6$) with respect to the ALPINE target. We refer to the source of this emission as Gal-A (RA: 10:01:13.82, Dec: +02:18:40.66), that is detected both in continuum and in line emission at 5σ and 12σ, respectively. Fig. 1 shows the continuum-subtracted moment-0 map of Gal-A (see section 2.4). Also shown are the synthesized beam with a size of 1.08" × 0.85" at P.A. = - 80°, and another galaxy (Gal-B) detected at 9σ in continuum only northwards of the offset emission (∼ 2" away from Gal-A when considering the peak position of the two emissions).

We show in Fig. 2 the spectrum of the emission line observed at the position of Gal-A; it is extracted from a circular region 2" wide, including the 2σ contours from the moment-0 map of the source. Using the *spectral profile tool* within the CASA viewer, we fit the line profile with a Gaussian function finding a full width at half maximum ($\mathrm{FWHM_{line}}$) of 308±34 km/s and a peak frequency at $\nu_{\rm peak} = 340.76$ GHz.

Though DC_665626 is detected in [CII] in spatial coincidence with its UV emission, we consider the possibility that the emission centred at the position of Gal-A is connected

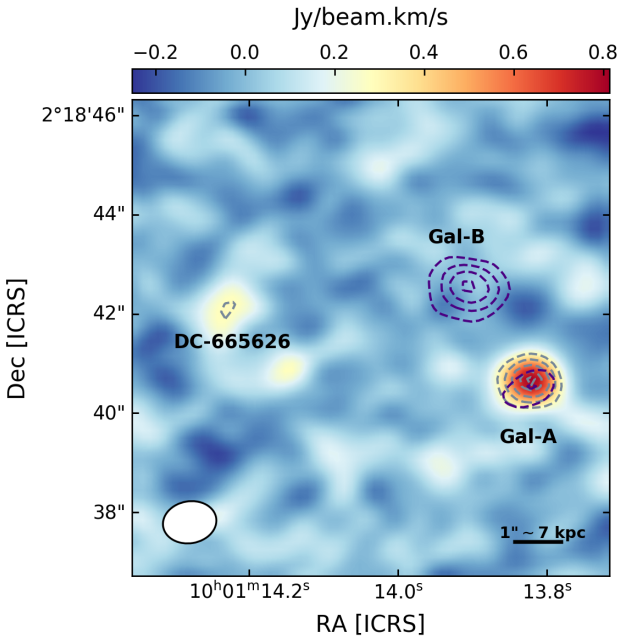


Figure 1. Continuum-subtracted moment-0 map of Gal-A. The ALPINE target DC_665626, Gal-A and Gal-B are labelled. Line and continuum emissions are shown with grey and purple contours starting from 4σ and 3σ (at step of 2σ), respectively. The white ellipse in the bottom left corner is the synthesized beam.

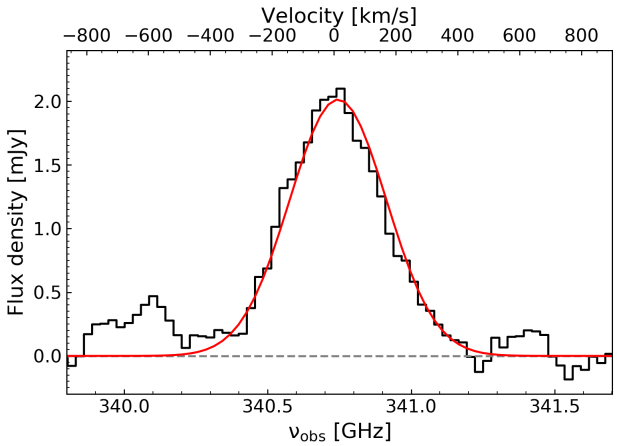


Figure 2. Emission line flux at the position of Gal-A (black histogram) as a function of the observed frequency. The solid red curve represents the gaussian fit on the line. The dashed grey line marks the zero-flux level. Also shown is the velocity offset on the top axis.

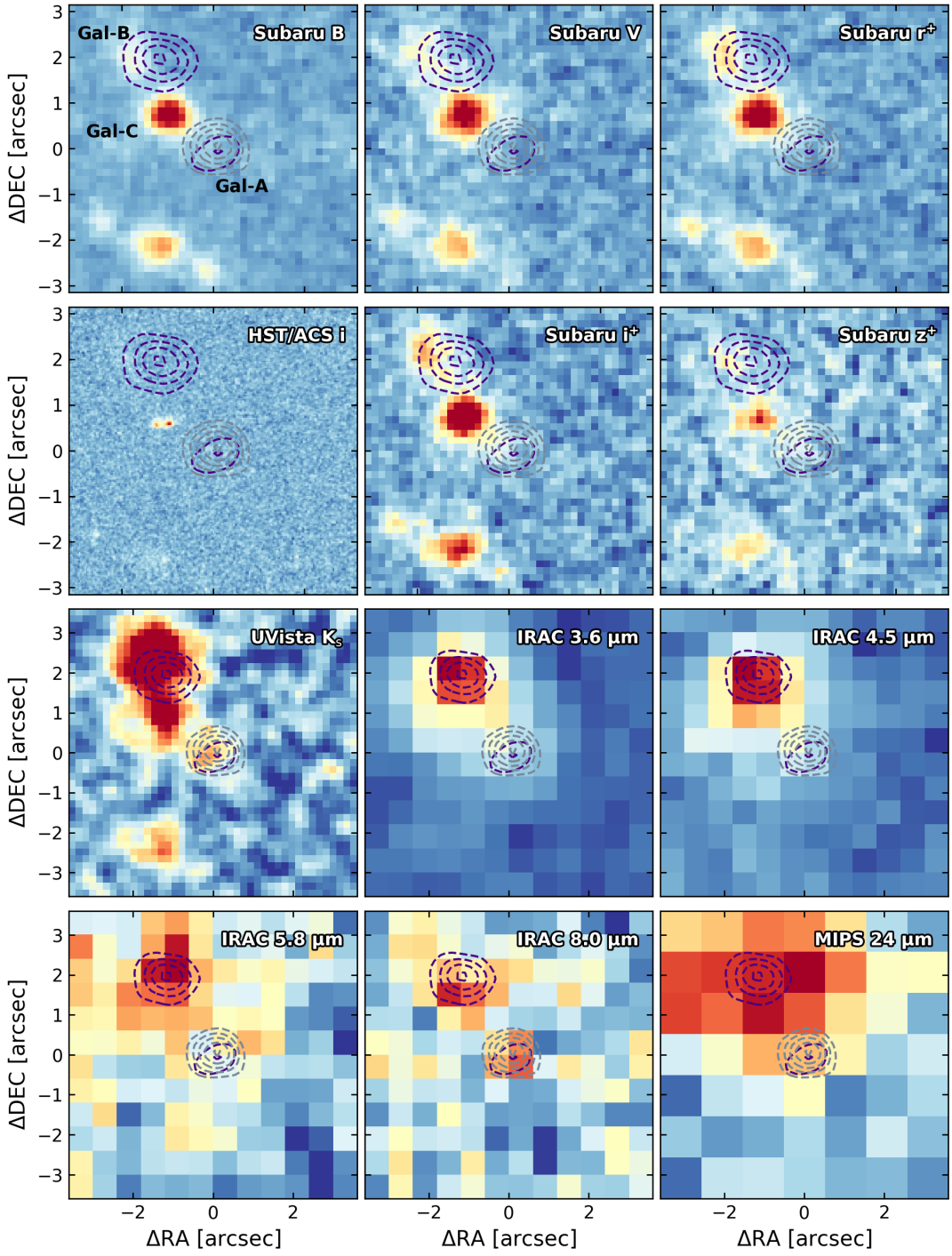


Figure 3. Cutouts centred on Gal-A in different photometric filters, from HST/ACS (Koekemoer et al. 2007) and Subaru, UltraVISTA and Spitzer (Capak et al. 2007; Laigle et al. 2016). Grey and purple contours are $> 3\sigma$ line and continuum emissions (at step of 2σ), respectively. Gal-A, Gal-B, and Gal-C are labelled in the upper-left plot of the figure. Wavelengths increase from the upper-left to the bottom-right corner.

with that of the ALPINE target. The displacement between [CII] and UV/Lyα emission has already been observed in high-redshift galaxies (Gallerani et al. 2012; Willott et al. 2015; Cassata et al. in prep.; but see also Bradač et al. 2017). It is also reproduced by radiative transfer simulations as a consequence of the strong stellar feedback which could quench the [CII] emission in the central region of the galaxies, allowing it to arise mostly from infalling or satellite clumps of neutral gas around them (Vallini et al. 2013; Maiolino et al. 2015). However, these models predict spatial offsets up to $\sim 1-2$ arcsec ($\sim 7-14$ kpc at the redshift of the target), well below the offset that we measure in this

case ($\gtrsim$ 6 arcsec). Therefore, we exclude that the observed ALMA emission at the position of Gal-A is directly linked to DC_665626.

2.3 Multi-wavelength photometry of Gal-A

As Gal-A lies in the COSMOS field (Laigle et al. 2016), we exploit all the available multi-wavelength photometry in order to identify the counterpart associated with the discovered emission. In Fig. 3 we present some cutouts centred on this galaxy in different photometric filters, from UV to FIR. Gal-B, that in the COSMOS2015 catalogue (Laigle et al. 2016) has a photometric redshift $z = 2.249^{+0.223}_{-0.151}$, is visible in most of the photometric bands. Another foreground galaxy, labelled Gal-C in Fig. 3, is well detected in the images from optical to NIR wavelengths, and has $z = 2.021^{+0.123}_{-0.116}$ in COSMOS2015. Conversely, Gal-A is not clearly visible in any optical filter except for the UltraVISTA K_s band, even if it is not listed as a detection in the UltraVISTA DR4 catalogue (McCracken et al. 2012).

More in detail, to reproduce the SED of Gal-A, we use observations in u^* band from MegaCam on CFHT, as well as the B, V, r^+, i^+, and z^{++} filters from Suprime-Cam on Subaru, in order to set an upper limit to the optical emission of the source. NIR constraints come from the J, H, and K_s bands from VIRCAM on the VISTA telescope. Finally, we obtain information on the SED up to $\sim$ 8 μm in the observed-frame from the IRAC channels on Spitzer. For each band, we centre a fixed aperture of 1.4" of diameter on Gal-A (enclosing the 3σ contours of the emission line detected by ALMA) and estimate its flux. The rms is computed as the average rms within several apertures (of 1.4" of diameter) placed in different regions of the sky, close to the source but away from evident emission. As expected, we don't find any significant detection of our source in the optical bands. Some marginal detections are present in the B, r^+, and i^+ filters, but they are all below 2σ and could be partially contaminated by the emission of Gal-C. For this reason, we consider the fluxes measured in these bands as upper limits. The same argument applies to the VISTA filters, except for the K_s band in which, as mentioned above, a faint emission arises at the position of Gal-A. Making use of `SExtractor` (Bertin & Arnouts 1996), we manage to deblend the analysed galaxy from the other two nearby sources obtaining an estimate of its apparent magnitude in this band. Through this analysis, Gal-A is detected at $\sim$ 2.3σ, with an AB magnitude $K_s = (24.8 \pm 0.5)$, which is very close to the corresponding 3σ limiting magnitude of $\sim$ 25 from the UltraVISTA DR4 catalogue.

Finally, a weak emission seems to arise at the position of Gal-A in the IRAC bands. However, as shown in Fig. 3, this could be partially contaminated by the emission of the two nearby galaxies at $z \sim 2$ in the 3.6 and 4.5 μm bands, while it seems to emerge from the background at 8.0 μm, where Gal-B and Gal-C become fainter. We find that, in the *Rainbow* catalogue (Pérez-González et al. 2008; Barro et al. 2011a,b), Gal-B and Gal-C have been deblended in all the four IRAC channels using the Subaru r band as a prior for the two sources, while no counterpart of Gal-A is present.

In order to extract the photometric information on Gal-A from the IRAC bands, we attempt a deblending procedure using the 2D GALFIT fitting algorithm (Peng et al. 2002).

Instrument /Telescope	Filter	Central λ [μm]	Observed flux [μJy]
MegaCam/CFHT	u^*	0.3783	$< 1.93 \times 10^{-2}$
Suprime-Cam /Subaru	B	0.4458	$< 4.12 \times 10^{-2}$
	V	0.5478	$< 6.90 \times 10^{-2}$
	r^+	0.6289	$< 6.88 \times 10^{-2}$
	i^+	0.7684	$< 9.32 \times 10^{-2}$
	z^{++}	0.9037	$< 2.92 \times 10^{-1}$
VIRCAM /VISTA	J	1.2495	$< 3.70 \times 10^{-1}$
	H	1.6553	$< 5.22 \times 10^{-1}$
	K_s	2.1640	$(4.25 \pm 1.85) \times 10^{-1}$
IRAC/Spitzer	ch1	3.5634	< 1.10
	ch2	4.5110	< 1.36
	ch3	5.7593	< 2.12
	ch4	7.9595	< 4.27

Table 1. Summary of available data for Gal-A in each photometric band used for the SED-fitting (see section 3.2). The first two columns are the instruments (with relative telescopes) and filters used. Central wavelength is the mean wavelength weighted by the transmission of the filter. In the last column, the fluxes (wich are all 2σ upper limits except for the K_s band) of Gal-A are shown. For the IRAC channels, we report the upper limits obtained by measuring the flux of Gal-A before the deblending procedure (see text). Except for the K_s detection (which is obtained with `SExtractor`), all the estimated photometry is directly obtained from the maps with an aperture of 1.4" of diameter centered on Gal-A.

We model Gal-B and Gal-C as point-like sources, using their optical positions and deblended fluxes from *Rainbow* as a first guess, and considering for each IRAC channel its typical PSF ($\sim 2''$). To obtain the Gal-A flux in each channel, we perform aperture photometry at the position of Gal-A in the residual maps[1]. We are aware that with this procedure we may underestimate the flux of Gal-A in the IRAC channels as we are spreading the global flux of the three components on only two sources. To account for this, when performing SED-fitting (see Section 3.2) we decide to consider IRAC fluxes ranging between the deblended (lower) and blended (higher) values. We find, however, that our conclusions do not depend on this assumption; in fact, we obtain similar results when using the deblended fluxes in the SED-fitting. As an alternative approach, we tried to fit a three-components model leaving as a free parameter the flux corresponding to Gal-A and using the ALMA continuum peak position as a prior. However, probably due to the small distance between the galaxies, the code is not able to perform the fit. Table 1 summarises the photometric information we obtain for Gal-A; this is exploited in section 3.2 to estimate the stellar mass of this galaxy.

[1] As we use a fixed aperture of 1.4" (which is smaller than the typical PSF of the IRAC channels) centred on Gal-A to obtain the photometry in each band, we apply aperture corrections to estimate the total fluxes in the IRAC filters. In particular, we divide the flux measured in these bands by 0.61, 0.59, 0.49 and 0.45, going from 3.6 to 8.0 μm

	ν_{rest} [GHz]	z_{gal}	log(L_{line}) [$L_\odot$]	log(L_{FIR}) [$L_\odot$]	log(SFR) [$M_\odot$/yr]
CO(9-8)	1036.9	2.043	8.04 ± 0.04	11.44 ± 0.50	1.45 ± 0.50
CO(10-9)	1152.0	2.381	8.20 ± 0.04	11.42 ± 0.50	1.43 ± 0.50
[CII]	1900.5	4.577	8.88 ± 0.04	11.38 ± 0.50	1.38 ± 0.50

Table 2. Summary of the physical parameters estimated for the three possible emission lines attributed to Gal-A. The first three columns report the considered emission line, its rest-frequency emission, and the redshift z_{gal} derived using the observed peak frequency, respectively. The fourth and fifth columns list the line luminosity (L_{line}) and the total infrared luminosity (L_{FIR}) for each emission lines, respectively. Finally, the last column report the SFRs, directly computed from the FIR luminosities following Kennicutt 1998.

2.4 Analysis of the serendipitous source

Since Gal-A shows no optical counterpart, we do not know a priori the nature of the emission line; it could be [CII] emission at a similar redshift of DC_665626 (i.e. $z \sim 4.6$), but also high-J CO transitions are expected ($J_{up} > 3$) at the observed frequencies in ALMA Band 7, although at lower redshift (Carilli & Walter 2013).

In this work, we consider only the two high-J CO transitions with $J_{up} = 9, 10$ which fall into the SPW of observation at $z \gtrsim 2$. Indeed, Ilbert et al. (2013) claim that galaxies at $z < 2$ (corresponding in our case to lower CO transitions) should be more easily detected in UV/optical filters, with a fraction always greater than 95% of sources detected in at least four photometric bands, from UV to NIR (Ilbert et al. 2006). Therefore, if our source was at $z < 2$, we would expect it to be visible in the optical bands shown in Fig. 3.

For these reasons, in this work we discuss the nature of Gal-A considering three transitions as possible interpretations for the observed emission: [CII] at $\nu_{rest} = 1900.5$ GHz, CO(9-8) at $\nu_{rest} = 1036.9$ GHz, and CO(10-9) at $\nu_{rest} = 1152.0$ GHz. As the observed emission line has a peak frequency of 340.76 GHz, Gal-A would be at redshift $z_{gal} = 4.577$, $z_{gal} = 2.043$ and $z_{gal} = 2.381$ for [CII], CO(9-8) and CO(10-9), respectively. Table 2 lists the considered transitions and their rest frequencies, as well as the corresponding redshift for Gal-A in the three cases.

To estimate the intensity of the line and continuum emissions from Gal-A, we separate these components using the CASA `IMCONTSUB` task; in particular, giving in input all the channels in the SPWs free of the emission line, this task creates a continuum map of the source and a continuum-subtracted cube. We then select all the consecutive channels having emission above $1\sigma_{spec}$ (i.e. the rms estimated from the line spectrum) encompassing the emission line in order to compute the moment-0 map with the CASA `IMMOMENTS` task.

The line and continuum fluxes are computed using the CASA `IMFIT` task. We define a region surrounding the emissions and then select only the pixels with a flux density larger than 2σ: since the size of the emission region is comparable with the clean beam size, we assume that the source is unresolved and we take the peak flux as the total flux. We obtain $S_{cont} = 245 \pm 24$ μJy and $S_{line}\Delta v = 1.19 \pm 0.11$ Jy km/s for the continuum and the line, respectively.

We derive the total infrared (between 8 and 1000 μm) luminosity of the source, in the three cases, assuming a shape of its SED from Magdis et al. (2012), and normalizing its flux to S_{cont}, which is the observed flux at $\sim 845-880$ μm; according to Kennicutt (1998), this luminosity also provides a good estimate of the obscured SFR. We obtain $\log(L_{FIR}/L_\odot) = 11.38 \pm 0.5$ in case of [CII] emission, $\log(L_{FIR}/L_\odot) = 11.44 \pm 0.5$ for CO(9-8), and $\log(L_{FIR}/L_\odot) = 11.42 \pm 0.5$ for CO(10-9) emissions. The uncertainties on the FIR luminosities are calculated by adding in quadrature the error on the continuum flux (~ 0.04 dex, which directly affects the L_{FIR} estimates), and a systematic error of 0.5 dex which takes into account possible variations in the luminosity caused by different FIR SED templates; as can be seen, this latter term dominates over the uncertainty on the flux. Following Eq. (4) in Kennicutt (1998), these FIR luminosities translate into SFRs ranging from 24 to 28 $M_\odot$/yr.[2] Finally, we estimate the line luminosities as in Solomon et al. (1992) using the following relation:

$$L_{line} = 1.04 \times 10^{-3}\, S_{line}\Delta v\, D_L^2\, \nu_{obs}\ [L_\odot], \qquad (1)$$

where D_L is the luminosity distance of the source in Mpc, and ν_{obs} the observed peak frequency in GHz. We thus obtain $\log(L_{[CII]}/L_\odot) = 8.88 \pm 0.04$, $\log(L_{CO}/L_\odot) = 8.04 \pm 0.04$ for CO(9-8) and $\log(L_{CO}/L_\odot) = 8.20 \pm 0.04$ for CO(10-9), where the uncertainties are computed by propagating the line flux error on the above equation. Table 2 reports all the above-mentioned physical quantities computed for Gal-A.

3 RESULTS

3.1 On the nature of the serendipitous source

With the only information of the ALMA Band 7 line and continuum, and with no detections in optical bands, unveiling the nature of Gal-A is a challenging task. We use the physical quantities estimated in section 2.4 to deduce plausible conclusions on this source.

Fig. 4 (left panel) shows the correlation between L_{CO} (for the (9-8) and (10-9) transitions) and L_{FIR} for a compilation of SFGs in literature, together with the expected position of Gal-A; the respective best-fitting lines on the individual data are also shown (solid lines, Liu et al. 2015). It is worth noting that the reported values are for local galaxies, spanning a FIR luminosity range between $\sim 10^8 - 10^{12}$ $L_\odot$. However, the empirical correlations continue to apply even including high-redshift galaxies (open diamonds in the figure); in this case indeed, as shown in Liu et al. (2015), the results of the fit do not significantly change. We then note

[2] We scale the SFR from Salpeter to Chabrier IMF by dividing by 1.7 (e.g. Zahid et al. 2012).

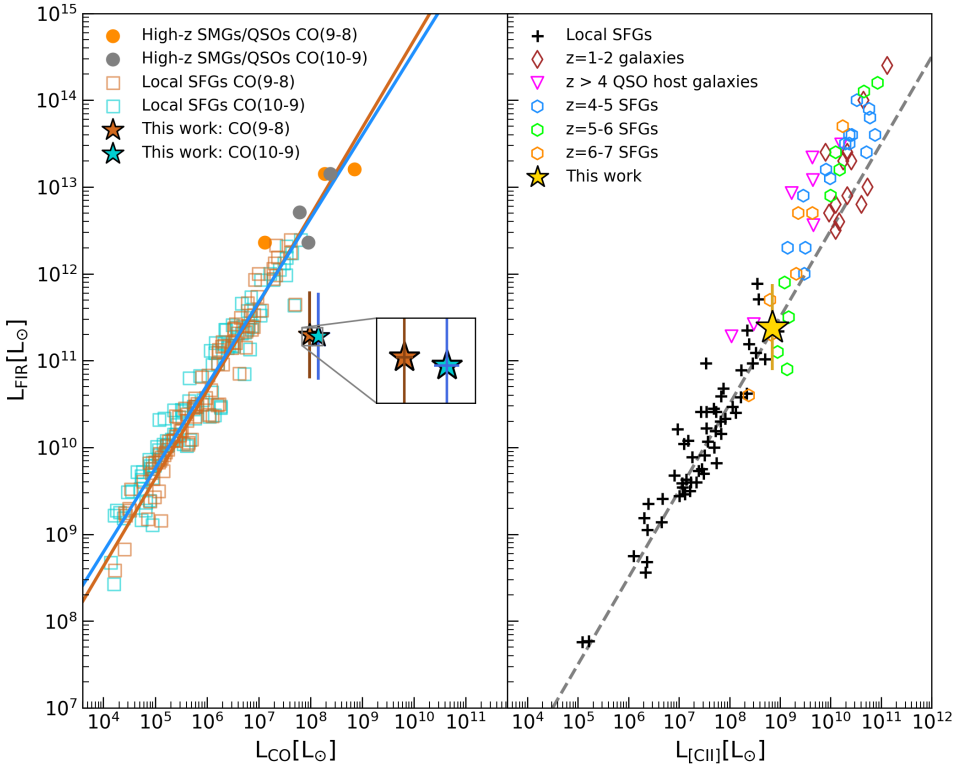


Figure 4. Left panel: empirical relations between CO(9-8) (solid brown line), CO(10-9) (solid blue line) and FIR luminosity (Liu et al. 2015) with overlaid the values for individual local galaxies as brown and blue open squares, respectively (Liu et al. 2015, private communication). The two stars are the values found for Gal-A in this work (same color legend). Error bars are estimated by propagating the error of the line flux on L_{CO}, and assuming a variation of 0.5 dex for L_{FIR}. Also shown are the values obtained for high-redshift sub-mm galaxies/quasi-stellar objects (QSOs) as the orange and grey filled circles, in case of CO(9-8) and CO(10-9) transitions, respectively (Carilli & Walter 2013; ALMA Partnership et al. 2015; Carniani et al. 2019). Right panel: [CII] as a function of FIR luminosity for several kinds of objects at different redshifts. Black crosses are local SFGs (Malhotra et al. 2001b); brown diamonds are $z = 1-2$ galaxies, including starburst- and AGN-dominated sources (Stacey et al. 2010); magenta triangles are $z = 4.1-7.1$ QSO host galaxies (Pety et al. 2004; Maiolino et al. 2005; Iono et al. 2006; Maiolino et al. 2009; Wagg et al. 2010; Willott et al. 2013); $z = 4-7$ SFGs are the cyan, green, and orange hexagons (Lagache et al. 2018). The dashed grey line represents the average [CII]-to-FIR ratio for local galaxies (Ota et al. 2014). The yellow star shows the position of our source. Error bars are estimated by propagating the error of the line flux on $L_{[CII]}$, and assuming a variation of 0.5 dex for L_{FIR}.

that the computed L_{FIR} of Liu et al. (2015) are integrated between $40-400$ μm, which is a smaller range with respect to the one adopted in this paper. In order to take this difference into account, we rescale the FIR luminosities of Gal-A in Fig. 4 to the same integration interval as in Liu et al. (2015), for consistency ($L_{FIR}^{8-1000}/L_{FIR}^{40-400} \sim 1.4$, on average). It can be seen that, for both possible CO transitions, our galaxy would be an outlier of the empirical relations found by Liu et al. (2015), if it was at $z \sim 2$. However, considering the large uncertainties on L_{FIR} (i.e. 0.5 dex), Gal-A could still be part of the lower envelope of local SFGs in the figure, tracing high-density regions ($n_{H2,crit} \sim 10^5 - 10^6$ cm^{-3}; Carilli & Walter 2013) where star formation may occur.

In the right panel of Fig. 4 we plot the [CII] luminosity as a function of L_{FIR} in case Gal-A was a [CII] emitter at $z \sim 4.6$, along with other results from several authors for different types of objects (e.g. Malhotra et al. 2001b, Stacey et al. 2010). Our source perfectly sits on the local SFGs relation, with $\log(L_{[CII]}/L_{FIR}) \sim -2.5$; possibly, this galaxy may belong to the high-redshift SFGs population which extends to $\log(L_{FIR}/L_\odot) \sim 11$. As previously said, the [CII] line is mostly produced by UV radiation field in star-forming regions (e.g. Cormier et al. 2015), then it can trace the SFR. Therefore, as the FIR emission marks out the SFR of a source, the relation between [CII] luminosity and L_{FIR} translates into a correlation between $L_{[CII]}$ and the SFR of a galaxy; Gal-A follows this relation, not showing the typical [CII] deficit which arises at $L_{FIR} > 10^{11}$ $L_\odot$ (Luhman et al. 1998; Malhotra 2001a; Luhman et al. 2003; Lagache et al. 2018).

These results suggest that our source, randomly detected in the DC_665626 field, may more likely be a strongly obscured [CII] emitter at high redshift. However, to validate this hypothesis, more data are needed.

3.2 Estimate of the stellar mass

We derive the stellar mass of Gal-A through SED-fitting using LePHARE (Arnouts et al. 1999; Ilbert et al. 2006).

We use a synthetic set of templates of SFGs based on

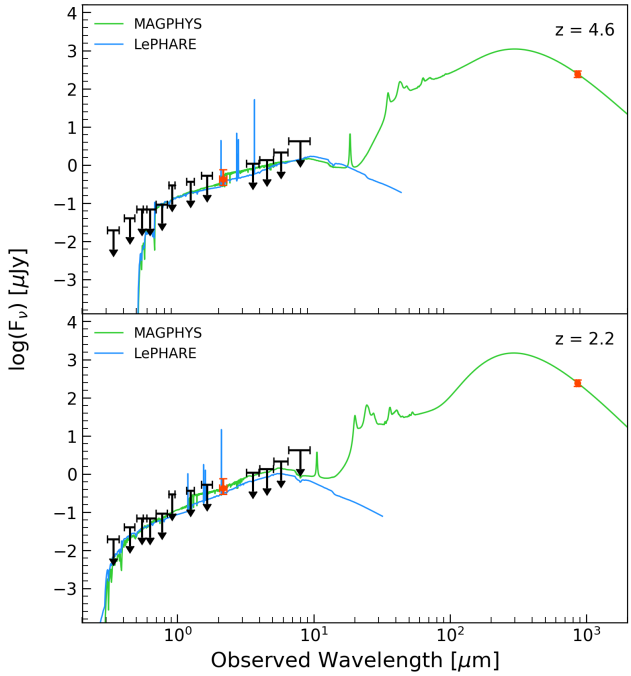


Figure 5. SEDs of Gal-A at $z = 4.6$ (top panel) and $z = 2.2$ (bottom panel). The green and blue curves are the best-fit models computed with the MAGPHYS and LePHARE codes, respectively. Upper limits on the flux, as reported in Table 1, are shown in black. The orange points with the error bars are the detection in the UltraVISTA K_s band and the observed ALMA continuum in Band 7.

stellar population synthesis models from Bruzual & Charlot (2003). We explore constant, exponentially declining (with $\tau = 0.1, 0.3, 1, 3$ Gyrs) and delayed (with $\tau = 0.1, 0.5, 1, 3$ Gyrs) SFHs. To account for metallicity dependence, we use models with solar ($Z_\odot$) and sub-solar ($0.2\ Z_\odot$) metallicity. We then account for dust attenuation using the Calzetti et al. (2000) attenuation law with a stellar $E_s(B-V)$ ranging from 0 to 0.7 in steps of 0.05. Following Ilbert et al. (2009), we also add the contribution of rest-frame UV and optical emission lines in the different filters. Finally, following Faisst et al. (2019), we perform the fit in flux density space and add systematic errors (depending on the filter) in order to avoid the χ^2 computation to be dominated by small errors.

Fig. 5 shows the SEDs obtained with LePHARE (blue curves) from the best-fit between the models and the photometry of Gal-A at $z = 4.6$ and $z = 2.2$. In the first case, the best-fit is given by an exponentially declining model with $\tau = 3.0$ Gyrs while, at $z = 2.2$, a delayed τ-model with $\tau = 0.5$ Gyrs better reproduces the observations.

Since Gal-A is very faint from optical to NIR wavelengths, we decide to perturb the flux in each filter by its relative rms to test the dependence of the fitting on the observed photometry of the galaxy. We thus run a Montecarlo simulation, building 1000 perturbed SEDs that we then refit, in order to obtain a better estimate of the above-mentioned physical parameters from their probability distributions. More in detail, we extract the perturbed flux in each band from a gaussian distribution centred on the measured flux and with standard deviation equal to the measured rms. We list our results in Table 3. At $z = 4.6$, these results point towards the solution for which Gal-A is a young, dusty SFG. Moreover, as can be seen, the SFR and the FIR luminosity are quite in agreement with the corresponding quantities in Table 2. Adopting the same procedure for the SED-fitting at $z = 2.2$, we find that Gal-A should be a less massive and dustier galaxy with respect to the previous case.

Physical parameters	z=2.2	z=4.6
$E_s(B-V)$	0.5 ± 0.1	0.4 ± 0.1
log(Age/Gyrs)	7.9 ± 0.3	7.8 ± 0.1
log(SFR/$M_\odot yr^{-1}$)	1.3 ± 0.4	2.1 ± 0.3
log($L_{FIR}/L_\odot$)	11.0 ± 0.1	11.6 ± 0.2
log($M_*/M_\odot$)	9.1 ± 0.2	9.7 ± 0.2

Table 3. Physical parameters estimated from the SED-fitting at $z = 2.2$ and $z = 4.6$. Each value represents the mean of the probability distribution obtained perturbing the photometry of Gal-A 1000 times and fitting that photometry with the models. The uncertainties are given by the 16th and 18th percentiles of the distributions.

We further compare the results obtained with LePHARE with the MAGPHYS code (da Cunha et al. 2008), in which we also include the observed ALMA continuum in Band 7. The best models that fit the observations are shown in Fig. 5 as the green curves. The results from the best-fit, both at $z = 2.2$ and $z = 4.6$, are very similar to those of LePHARE within the uncertainties. This reassures us about the robustness of our estimates.

With the stellar mass obtained from the SED-fitting and the SFR measured from the FIR luminosity of the source, we determine the position of Gal-A along the MS of SFGs. In Fig. 6 we show the MS relations, assuming a Chabrier IMF, at $z = 2.2$ (left panel) and $z = 4.6$ (right panel) obtained by Speagle et al. (2014) combining measurements from previous works in literature. Should the source be at $z = 2.2$, it would lie $\sim 2\sigma$ above the MS, towards the region populated by starburst galaxies.

Whether the source is at $z = 4.6$, instead, it would sit on its corresponding MS. In this case, we also show the location of the ALPINE sample (in the redshift range $4.4 \leq z \leq 4.6$) in the figure. The ALPINE galaxies have ages in the range $7.8 \lesssim \log(\mathrm{Age}) \lesssim 9.0$ and $E_s(B-V)$ between 0 and 0.5 (Faisst et al. 2019). Gal-A has a similar age to those estimated for the ALPINE targets; moreover, its SFR and M_* are comparable with those of the ALPINE sources and place it along the MS at $z = 4.6$. However, the mean $E_s(B-V)$ of the ALPINE galaxies is ~ 0.1, while Gal-A has $E_s(B-V) \sim 0.4$, lying on the tail of the distribution of the color excess, and making it undetected in the optical bands. In this scenario, we should expect an entire population of optically-invisible SFGs, still to be observed, which might significantly contribute to the cosmic SFRD at early times.

3.3 Estimate of the dynamical mass

In this paragraph we attempt an estimate of the galaxy dynamical mass (M_{dyn}) obtained from the FWHM of the

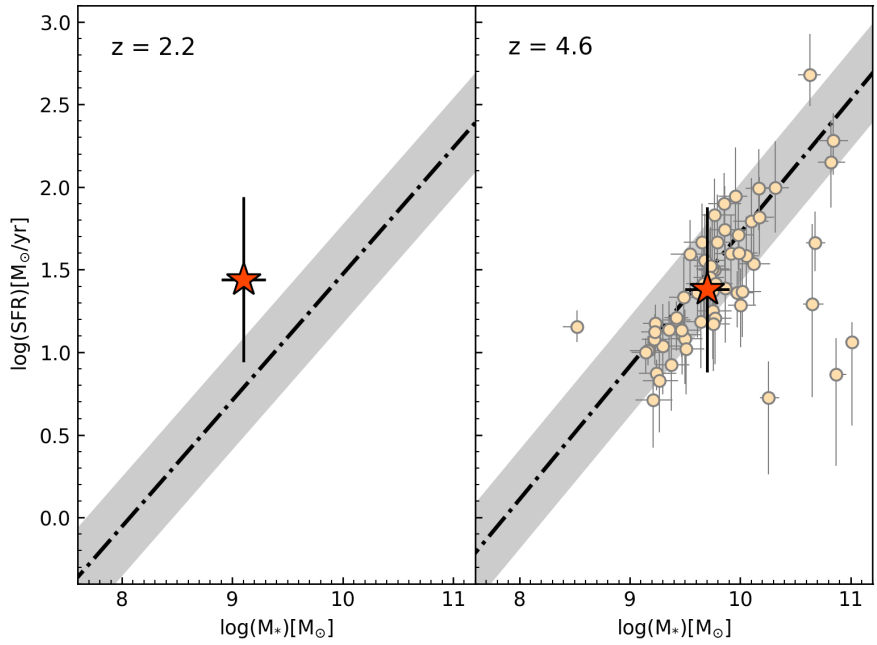


Figure 6. Star-forming MS relations (dot-dashed lines; Speagle et al. 2014) at redshift 2.2 (left panel) and 4.6 (right panel). The grey bands indicate the scatter from the MS (±0.3 dex width). The orange stars represent the positions of our source in the diagram, given by the estimated stellar mass from the SEDfitting and the SFR from the FIR luminosity of Gal-A. For the case at $z = 4.6$, we also show the positions of the ALPINE galaxies at $4.4 \leq z \leq 4.6$ (small circles).

observed emission line. Following Wang et al. (2013), we assume a rotating disk geometry for the gas as a first approximation; in this way, $M_{dyn} = 1.16 \times 10^5\, v_{cir}^2\, D$, where $v_{cir} = 0.75\, FWHM_{line}/\sin(i)$ is the circular velocity of the gas disk in km/s (with i the inclination angle between the gas disk and the line of sight), and D is the disk diameter in kpc. Since Gal-A is not resolved, we take the FWHM of the major axis of the 2D Gaussian fitted to the emission line, as the size of our galaxy (1.06 ± 0.04 arcsec, which corresponds to 7.09 ± 0.27 kpc at $z \sim 4.6$, and to 8.99 ± 0.34 kpc at $z \sim 2.2$). We derive dynamical masses (uncorrected for galaxy inclination) of $M_{dyn}\sin^2(i) = 4.4 \times 10^{10}\ M_\odot$ and $5.6 \times 10^{10}\ M_\odot$ for $z = 4.6$ and $z = 2.2$ respectively, with a 25% uncertainty obtained from individual errors on the $FHWM_{line}$ and on the size of the source. Following Capak et al. (2015), we assume the two values for the inclination angle $\sin(i) = 0.45$ and $\sin(i) = 1$, ranging from a nearly face-on to an edge-on disk. When $\sin(i) = 1$, the previous dynamical masses remain unchanged; however, in the case with $\sin(i) = 0.45$, M_{dyn} increases of a factor 5. This reflects the large uncertainties on the size and geometry of the source, which cannot be well constrained with the current data and our poor resolution.

Furthermore, this approximation could cease to be valid in case the stellar mass of the source is smaller than the mass threshold above which galaxies are thought to form ordered disks. For instance, Simons et al. (2015) found a so-called "mass of disk formation" of $\log(M_*/M_\odot) = 9.5$ above which the majority of the galaxies of their sample are rotation-dominated; below this threshold there is instead a large scatter and the galaxies could be either rotation-dominated disks and asymmetric or compact galaxies without any sign of rotation. At $z = 2.2$, Gal-A should have $\log(M_*/M_\odot) = 9.1$, therefore it is prone to this kind of issue.

For comparison, we also run the 3D-BAROLO algorithm (3D-Based Analysis of Rotating Objects from Line Observations; Di Teodoro & Fraternali 2015) on the continuum-subtracted data cube to obtain a more accurate estimate of the dynamical mass. This code creates synthetic 3D observations of the galaxy and compares them with the input cube, finding the kinematical and geometrical parameters which best describe the data. It is particularly useful to retrieve information on low-resolution data where the kinematics is biased by the size of the beam, as in this case. We find $\log(M_{dyn}/M_\odot) = 10.4 \pm 1.0$ for $z = 4.6$ and $\log(M_{dyn}/M_\odot) = 10.5 \pm 1.0$ for $z = 2.2$. These results are quite in agreement with the former, given the large error on M_{dyn}. In particular, at both redshifts, $M_{dyn}/M_* > 1$, likely indicating that the galaxy has recently begun forming stars, resulting in small stellar masses and large gas fractions. However, given the large uncertainties on the dynamical mass, this result is not conclusive.

4 DISCUSSION

In light of the above results, it seems more likely that Gal-A is a dust-obscured galaxy at $z = 4.6$. From the [CII]/FIR diagnostic, our source presents similar properties to a large population of SFGs in literature. In addition, the SED-fitting reveals a large dust attenuation as expected for such an obscured galaxy, and places Gal-A along the MS at $z \sim 4.6$. Nevertheless, we cannot exclude the possibility that the observed emission line is associated to a dusty, less mas-

sive source at $z \sim 2.2$, with a $\sim 2\sigma$ scatter from the MS and having relatively higher CO luminosities than those typical of local SFGs and high-z sub-millimeter galaxies. In this latter case, the (spectroscopic) redshift of Gal-A would also be comparable with the (photometric) redshifts of Gal-B and Gal-C, maybe suggesting the presence of an on-going merging at that epoch. However, to test this hypothesis, more kinematic information is needed.

In the most likely scenario in which Gal-A is at $z \sim 4.6$, it may be part of the same dark matter halo of DC_665626. In this case, we can assume a stellar mass – halo mass (SMHM) relationship in order to estimate some physical properties of the halo. There are several ways to derive this relation; e.g. Behroozi et al. (2010, 2013) used the abundance matching technique to explore the SMHM relation out to $z \sim 8$ assuming that the most massive galaxies are monotonically assigned to the most massive halos. Another approach is the Halo Occupation Distribution modeling which assumes that the number of galaxies in a given dark matter halo depends only on the halo mass; Harikane et al. (2016) used this method to reproduce the SMHM relation out to $z = 7$, obtaining results in agreement with Behroozi et al. (2013). In particular, since Gal-A has a larger stellar mass than DC_665626, we can suppose that the ALPINE target is a satellite galaxy of our serendipitous source embedded in its dark matter halo. In this case, from the stellar mass of Gal-A (i.e. $\log(M_*/M_\odot) = 9.7 \pm 0.2$), the previously discussed models predict a halo mass between $\log(M_h/M_\odot) \sim 11.5$ and $\log(M_h/M_\odot) \sim 11.7$. Using the empirical model by Mashian et al. (2015), which links the SFR of the central galaxy to its host halo mass via abundance matching techniques, M_h also translates into an SFR between ~ 20 and $40\ M_\odot yr^{-1}$, in agreement, within the uncertainties, with the value estimated from the FIR continuum for Gal-A, i.e. SFR $\sim 24\ M_\odot yr^{-1}$. Exploiting these information and following Lapi et al. (2018), we compute the virial radius of the halo as $R_H \equiv [3M_H/4\pi\rho_c\Delta_H E_z]^{1/3}$, where $\rho_c \approx 2.8 \times 10^{11} h^2\ M_\odot/Mpc^3$ is the critical density, $\Delta_H \simeq 18\pi^2 + 82[\Omega_m(1+z)^3/E_z - 1] - 39[\Omega_m(1+z)^3/E_z - 1]^2$ is the non-linear density contrast at collapse, and $E_z = \Omega_\Lambda + \Omega_m(1+z)^3$ is a redshift dependent factor; we obtain $R_H \sim 39 - 45$ kpc. Comparing this result to the observed spatial offset between our source and DC_665626 (~ 40 kpc), we may conclude, according to this scenario, that the main ALPINE target could be a low mass satellite in the dark matter halo of Gal-A.

It is worth noting that we obtain similar results even in the opposite case in which Gal-A is a satellite galaxy of DC_665626. Following the same procedure explained above, and since DC_665626 has $\log(M_*/M_\odot) \sim 9.2$, we obtain $\log(M_h/M_\odot) \sim 11.4$ and $\log(SFR/[M_\odot yr^{-1}]) \sim 1.0$ (which is consistent with the SFR of the ALPINE target obtained through SED-fitting). In turn, this provides $R_H \sim 36$ kpc, which is again comparable with the observed offset between the two galaxies.

Finally, Gal-A may also be part of the massive protocluster of galaxies PCI J1001+0220 located at $z = 4.57$ in the COSMOS field (Lemaux et al. 2018). In fact, our source lies well inside the 2 Mpc boundary used for spectroscopic membership in that work, with a systemic velocity offset < 350 km/s. This strengthens the hypothesis that this source is at $z \sim 4.6$.

5 SUMMARY AND CONCLUSIONS

In this paper we present the characterisation of Gal-A, a galaxy serendipitously discovered in one of the ALPINE pointings. This source is detected both in line and continuum and does not show any optical counterpart, from UV to FIR, except for the K_s band from UltraVISTA (DR4). This leads to high uncertainties on the real nature of the observed emission line, i.e. [CII] at $z_{gal} = 4.577$, CO(9-8) or CO(10-9) at $z_{gal} = 2.043$ and 2.381, respectively.

Although we cannot definitively exclude that Gal-A is a dust-obscured galaxy at $z \sim 2.2$, the analysis undertaken in this work suggests that this source is more likely a $z \sim 4.6$ MS SFG missed by UV/optical surveys because of its high level of dust-obscuration. Moreover, at this epoch, several dusty galaxies without optical/NIR detections have been yet confirmed, mostly as extreme starbursts (e.g. Riechers et al. 2013, 2017; Alcalde Pampliega et al. 2019); Gal-A could be part of this elusive population of sources, with a smaller luminosity and/or mass. In this last case, we compute an SFR $\sim 24\ M_\odot$/yr from the FIR luminosity, $\log(M_*/M_\odot) \sim 9.7$ and an age of ~ 70 Myrs from Montecarlo simulations on the SED-fitting procedure.

Whether the emission comes from CO or [CII], both the cases presented above are undoubtedly interesting. If it was at $z \sim 2.2$, our galaxy would increase the sample of high-J CO emitters at high redshift, leading to a more in-depth study of the excitation conditions of the molecular gas in these sources; only a handful of these kind of objects has been detected so far, and most of them seem to be associated with active galactic nuclei (AGNs) activities (Weiß et al. 2007; Riechers et al. 2011, 2013). Should the serendipitous emission be [CII] instead, we would identify a SFG invisible to optical-NIR observations. [CII] emission traces recent star formation in the galaxy, and the ALPINE survey will allow us to quantify how many similar objects to the one analysed in this work we will be able to discover. In fact, among the serendipitous sources found in ALPINE, there is a high fraction of objects without UV/optical counterparts (Loiacono et al. in prep.). Thanks to ALPINE, we are now able to estimate the overall contribution of these dust-obscured galaxies to the SFRD in the early Universe.

Eventually, we plan to spectroscopic follow-up this source in order to firmly establish the nature of its emission line. For instance, ALMA observations in Band 6 could reveal [NII] emission at 205 μm rest-frame if the galaxy is at $z \sim 4.6$; in this case the ratio [CII]/[NII] would also provide the fraction of [CII] emission arising from the ionised gas, i.e. from star-forming regions (Oberst et al. 2006, 2011; Zhao et al. 2010). X-shooter at the Very Large Telescope (VLT) could also be useful to unveil the redshift of this source by observing [OII] emission at $z = 4.6$, or even Hα emission redshifted in the NIR region of the spectrum at $z \sim 2.2$. However, these observations could be hampered by the large $E_s(B-V)$ found for this source which makes it invisible in optical filters. Finally, the Near-Infrared Spectrograph (NIRSpec) on the James Webb Space Telescope (JWST) will be a powerful facility for the follow-up of this kind of sources as well.

ACKNOWLEDGEMENTS

This paper is based on data obtained with the ALMA observatory, under the Large Program 2017.1.00428.L. ALMA is a partnership of ESO (representing its member states), NSF (USA) and NINS (Japan), together with NRC (Canada), MOST and ASIAA (Taiwan), and KASI (Republic of Korea), in cooperation with the Republic of Chile. The Joint ALMA Observatory is operated by ESO, AUI/NRAO and NAOJ. Based on data products from observations made with ESO Telescopes at the La Silla Paranal Observatory under ESO programme ID 179.A-2005 and on data products produced by CALET and the Cambridge Astronomy Survey Unit on behalf of the UltraVISTA consortium. This work has made use of the Rainbow Cosmological Surveys Database, which is operated by the Centro de Astrobiología (CAB/INTA), partnered with the University of California Observatories at Santa Cruz (UCO/Lick,UCSC). We thank D. Liu and collaborators for providing us individual values of CO and FIR luminosities estimated in their work. S.B., A.C., C.G., F.L., F.P., G.R., and M.T. acknowledge the support from grant PRIN MIUR 2017. L.V. acknowledges funding from the European Union's Horizon 2020 research and innovation program under the Marie Sk lodowska-Curie Grant agreement No. 746119. D.R. acknowledges support from the National Science Foundation under grant numbers AST-1614213 and AST-1910107 and from the Alexander von Humboldt Foundation through a Humboldt Research Fellowship for Experienced Researchers. G.C.J. acknowledges ERC Advanced Grant 695671 "QUENCH" and support by the Science and Technology Facilities Council (STFC). S.F. is supported by the Cosmic Dawn Center of Excellence founded by the Danish National Research Foundation under the grant No. 140.

REFERENCES

Alcalde Pampliega, B., Pérez-González, P. G., Pablo, G., et al. 2019, ApJ, 876, 135
ALMA Partnership, Vlahakis, C., Hunter, T. R., et al. 2015, ApJ, 808, 4
Álvarez-Márquez, J., Burgarella, D., Heinis, S., et al. 2016, A&A, 587, 122
Aravena, M., Decarli, R., Walter, F., et al. 2016, ApJ, 833, 71
Arnouts, S., Cristiani, S., Moscardini, L., et al. 1999, MNRAS, 310, 540
Barro, G., Pérez-González, P. G., Gallego, J., et al. 2011a, ApJS, 193, 13
Barro, G., Pérez-González, P. G., Gallego, J., et al. 2011b, ApJS, 193, 30
Behroozi, P. S., Conroy, C., & Wechsler, R. H. 2010, ApJ, 717, 379
Behroozi, P. S., Wechsler, R. H., & Conroy, C. 2013, ApJ, 770, 57
Bertin, E. & Arnouts, S. 1996, A&AS, 117, 393
Blain, A. W., Smail, I., Ivison, R. J., et al. 2002, Phys. Rep., 369, 111
Bouwens, R. J., Illingworth, G. D., Labbe, I., et al. 2011, Nature, 469, 504
Bouwens, R. J., Illingworth, G. D., Oesch, P. A., et al. 2012a, ApJ, 754, 83
Bouwens, R. J., Illingworth, G. D., Oesch, P. A., et al. 2012b, ApJ, 752, 5
Bouwens, R. J., Aravena, M., Decarli, R., et al. 2016, ApJ, 833, 72
Bradač, M., Garcia-Appadoo, D., Huang, K.-H., et al. 2017, ApJ, 836, 2
Bruzual, G., & Charlot, S. 2003, MNRAS, 344, 1000
Calzetti, D., Armus, L., Bohlin, R. C., et al. 2000, ApJ, 533, 682
Capak, P. L., Aussel, H., Ajiki, M., et al. 2007, ApJS, 172, 99
Capak, P. L., Carilli, C. L., Lee, N., et al. 2008, ApJ, 681, 53
Capak, P. L., Carilli, C., Jones, G., et al. 2015, arXiv:1503.07596
Cardamone, C. N., van Dokkum, P. G., Urry, C. M., et al. 2010, ApJS, 189, 270
Carilli, C. L., & Walter, F. 2013, ARA&A, 51, 105
Carniani, S., Gallerani, S., Vallini, L., et al. 2019, MNRAS, 489, 3939
Casey, C. M., Berta, S., Béthermin, M., et al. 2012, ApJ, 761, 140
Casey, C. M., Narayanan, D., & Cooray, A. 2014, Phys. Rep., 541, 45
Castellano, M., Sommariva, V., Fontana, A., et al. 2014, A&A, 566, 19
Chabrier, G. 2003, PASP, 115, 763
Cormier, D., Lebouteiller, V., Madden, S. C., et al. 2012, A&A, 548, 20
Cormier, D., Madden, S. C., Lebouteiller, V., et al. 2015, A&A, 578, 53
da Cunha, E., Charlot, S., & Elbaz, D. 2008, MNRAS, 388, 1595
Daddi, E., Dickinson, M., Morrison, G., et al. 2007, ApJ, 670, 156
Daddi, E., Dannerbauer, H., Stern, D., et al. 2009, ApJ, 694, 1517
De Looze, I., Cormier, D., Lebouteiller, V., et al. 2014, A&A, 568, 62
Di Teodoro, E. M., & Fraternali, F. 2015, MNRAS, 451, 3021
Dunlop, J. S., McLure, R. J., Yamada, T., et al. 2004, MNRAS, 350, 769
Faber, S. M., Phillips, A. C., Kibrick, R. I., et al. 2003, in Society of Photo-Optical Instrumentation Engineers (SPIE) Conference Series, Vol. 4841, Instrument Design and Performance for Optical/Infrared Ground-based Telescopes, ed. M. Iye & A. F. M. Moorwood, 1657-1669
Faisst, A. L., Schaerer, D., Lemaux, B. C., et al. 2019, arXiv:1912.01621
Gallerani, S., Maiolino, R., Juarez, Y., et al. 2010, A&A, 532, 85
Gallerani, S., Neri, R., Maiolino, R., et al. 2012, A&A, 543, 114
Genzel, R., Tacconi, L. J., Lutz, D., et al. 2015, ApJ, 800, 20
Giavalisco, M. 2002, ARA&A, 40, 579
Giavalisco, M., Ferguson, H. C., Koekemoer, A. M., et al. 2004, ApJ, 600, 93
Harikane, Y., Ouchi, M., Ono, Y., et al. 2016, ApJ, 821, 123
Hasinger, G., Capak, P., Salvato, M., et al. 2018, ApJ, 858, 77
Hollenbach, D. J., & Tielens, A. G. G. M. 1999, RvMP, 71, 173
Huang, J.-S., Rigopoulou, D., Magdis, G., et al. 2014, ApJ, 784, 52
Ilbert, O., Arnouts, S., McCracken, H. J., et al. 2006, A&A, 457, 841
Ilbert, O., Capak, P., Salvato, M., et al. 2009, ApJ, 690, 1236
Ilbert, O., McCracken, H. J., Le Fèvre, O., et al. 2013, A&A, 556, 55
Iono, D., Yun, M. S., Elvis, M., et al. 2006, ApJ, 645, 97
Lapi, A., Pantoni, L., Zanisi, L., et al. 2018, ApJ, 857, 22
Kaufman, M. J., Wolfire, M. G., Hollenbach, D. J., & Luhman, M. L. 1999, ApJ, 527, 795
Kennicutt, R. C. 1998, ARA&A, 36, 189
Koekemoer, A. M., Aussel, H., Calzetti, D. et al. 2007, ApJS, 172, 196
Koekemoer, A. M., Faber, S., Ferguson, H. et al. 2011, ApJS, 197, 36
Lagache, G., Cousin, M., & Chatzikos, M. 2018, A&A, 609, 130
Laigle, C., McCracken, H. J., Ilbert, O., et al. 2016, ApJS, 224, 24
Le Fèvre, O., Saisse, M., Mancini, D., et al. 2003, In Proc.

SPIE, Vol. 4841, Instrument Design and Performance for Optical/Infrared Ground-based Tele-scopes, ed. M. Iye & A. F. M. Moorwood, 1670–1681
Le Fèvre, O., Tasca, L. A. M., Cassata, P., et al. 2015, A&A, 576, 79
Le Fèvre, O., Béthermin, M., Faisst, A., et al. 2019, arXiv:1910.09517
Lemaux, B. C., Le Fèvre, O., Cucciati, O., et al. 2018, A&A, 615, 77
Lilly, S. J., Le Fèvre, O., Hammer, F., & Crampton, D. 1996, ApJ, 460, 1
Liu, D., Gao, Y., Isaak, K., et al. 2015, ApJ, 810, 14
Luhman, M. L., Satyapal, S., Fischer, J., et al. 1998, ApJ, 504, 11
Luhman, M. L., Satyapal, S., Fischer, J., et al. 2003, ApJ, 594, 758
Madau, P., & Dickinson, M. 2014, ARA&A, 52, 415
Madden, S. C., Poglitsch, A., Geis, N., et al. 1997, ApJ, 483, 200
Magdis, G. E., Daddi, E., Béthermin, M., et al. 2012, ApJ, 760, 6
Maiolino, R., Cox, P., Caselli, P., et al. 2005, A&A, 440, 51
Maiolino, R., Caselli, P., Nagao, T., et al. 2009, A&A, 500, 1
Maiolino, R., Carniani, S., Fontana, A., et al. 2015, MNRAS, 452, 54
Malhotra, S. 2001, ESASP, 460, 155
Malhotra, S., Kaufman, M. J., Hollenbach, D., et al. 2001, ApJ, 561, 766
Mashian, N., Oesch, P., & Loeb, A. 2015, arXiv:1507.00999
McCracken, H. J., Milvang-Jensen, B., Dunlop, J., et al. 2012, A&A, 544, 156
McMullin, J. P., Waters, B., Schiebel, D., Young, W., & Golap, K. 2007, in Astronomical Society of the Pacific Conference Series, Vol. 376, Astronomical Data Analysis Software and Systems XVI, ed. R. A. Shaw, F. Hill, & D. J. Bell, 127
Naab, T., & Ostriker, J. P. 2017, ARA&A, 55, 59
Novak, M., Smolčić, V., Delhaize, J., et al. 2017, A&A, 602, 5
Oberst, T. E., Parshley, S. C., Stacey, G. J., et al. 2006, ApJ, 652, 125
Oberst, T. E., Parshley, S. C., Nikola, T., et al. 2011, ApJ, 739, 100
Oesch, P. A., Bouwens, R. J., Illingworth, G. D., et al. 2015, ApJ, 808, 104
Ota, K., Walter, F., Ohta, K., et al. 2014, ApJ, 792, 34
Pavesi, R., Riechers, D. A., Capak, P. L., et al. 2016, ApJ, 832, 151
Pavesi, R., Riechers, D. A., Sharon, C. E., et al. 2018, ApJ, 861, 43
Peng, C. Y., Ho, L. C., Impey, C. D., & Rix, H.-W. 2002, AJ, 124, 266
Pentericci, L., Vanzella, E., Castellano, M., et al. 2018, A&A, 619, 147
Pety, J., Beelen, A., Cox, P., et al. 2004, A&A, 428, 21
Pérez-González, P. G., Rieke, G. H., Villar, V., et al. 2008, ApJ, 675, 234
Planck Collaboration 2018, arXiv:1807.06209
Renzini, A. 2006, ARA&A, 44, 141
Riechers, D. A., Capak, P. L., Carilli, C. L., et al. 2010, ApJ, 720, 131
Riechers, D. A., Walter, F., Carilli, C. L., et al. 2011, ApJ, 726, 50
Riechers, D. A., Bradford, C. M., Clements, D. L., et al. 2013, Nature, 496, 329
Riechers, D. A., Leung, T. K. D., Ivison, R. J., et al. 2017, ApJ, 850, 1
Rodighiero, G., Daddi, E., Baronchelli, I., et al. 2011, ApJ, 739, 40
Santini, P., Castellano, M., Fontana, A., et al. 2016, A&A, 596, 75
Santini, P., Fontana, A., Castellano, M., et al. 2017, ApJ, 847, 76
Schenker, M. A., Robertson, B. E., Ellis, R. S., et al. 2013, ApJ, 768, 196
Scoville, N., Aussel, H., Brusa, M., et al. 2007, ApJS, 172, 1
Scoville, N., Abraham, R. G., Aussel, H., et al. 2007, ApJS, 172, 38
Scoville, N., Faisst, A., Capak, P., et al. 2015, ApJ, 800, 108
Scoville, N., Sheth, K., Aussel, H., et al. 2016, ApJ, 820, 83
Silk, J., & Mamon, G. A. 2012, RAA, 12, 917
Silverman, J. D., Daddi, E., Rodighiero, G., et al. 2015, ApJ, 812, 23
Simons, R. C., Kassin, S. A., Weiner, B. J., et al. 2015, MNRAS, 452, 986
Solomon, P. M., Downes, D., & Radford, S. J. E. 1992, ApJ, 398, 29
Speagle, J. S., Steinhardt, C. L., Capak, P. L., & Silverman, J. D. 2014, ApJS, 214, 15
Stacey, G. J., Geis, N., Genzel, R., et al. 1991, ApJ, 373, 423
Stacey, G. J., Hailey-Dunsheath, S., Ferkinhoff, C., et al. 2010, ApJ, 724, 957
Vallini, L., Gallerani, S., Ferrara, A., & Baek, S. 2013, MNRAS, 433, 1567
Vallini, L., Gallerani, S., Ferrara, A., et al. 2015, ApJ, 813, 36
Wagg, J., Carilli, C. L., Wilner, D. J., et al. 2010, A&A, 519, 1
Walter, F., Decarli, R., Carilli, C., et al. 2012, Nature, 486, 233
Wang, R., Wagg, J., Carilli, C. L., et al. 2013, ApJ, 773, 44
Wang, T., Elbaz, D., Schreiber, C., et al. 2016, ApJ, 816, 84
Weiß, A, Downes, D., Neri, R., et al. 2007, A&A, 467, 955
Williams, C. C., Labbe, I., Spilker, J., et al. 2019, ApJ, 884, 154
Willott, C. J., Omont, A., & Bergeron, J. 2013, ApJ, 770, 13
Willott, C. J., Carilli, C. L., Wagg, J., & Wang, R. 2015, ApJ, 807, 180
Wolfire, M. G., McKee, C. F., Hollenbach, D., & Tielens, A. G. G. M. 2003, ApJ, 587, 278
Zahid, H. J., Dima, G. I., Kewley, L. J., et al. 2012, ApJ, 757, 54
Zanella, A., Daddi, E., Magdis, G., et al. 2018, MNRAS, 481, 1976
Zhao, Y., Lu, N., Xu, C. K., et al. 2016, ApJ, 819, 69
Zhu, Y.-N., Wu, H., Li, H.-N., & Cao, C. 2010, RAA, 10 329

This paper has been typeset from a TEX/LATEX file prepared by the author.

AFFILIATIONS

[1] *Dipartimento di Fisica e Astronomia, Università di Padova, Vicolo dell'Osservatorio 3, I-35122, Padova, Italy*
[2] *INAF–Osservatorio Astronomico di Padova, Vicolo dell'Osservatorio 5, I-35122, Padova, Italy*
[3] *Department of Physics, University of California, Davis, One Shields Ave., Davis, CA 95616, USA*
[4] *Aix Marseille Univ, CNRS, CNES, LAM, Marseille, France*
[5] *IPAC, California Institute of Technology, 1200 East California Boulevard, Pasadena, CA 91125, USA*
[6] *The Cosmic Dawn Center, University of Copenhagen, Vibenshuset, Lyngbyvej 2, DK-2100 Copenhagen, Denmark*
[7] *Niels Bohr Institute, University of Copenhagen, Lyngbyvej 2, DK-2100 Copenhagen, Denmark*
[8] *Observatoire de Genève, Université de Genève 51 Ch. des Maillettes, 1290 Versoix, Switzerland*
[9] *Institut de Recherche en Astrophysique et Planétologie - IRAP, CNRS, Université de Toulouse, UPS-OMP, 14, avenue E. Belin,*
[10] *Kavli Institute for the Physics and Mathematics of the Universe, The University of Tokyo Kashiwa, Chiba 277-8583, Japan*
[11] *Department of Astronomy, School of Science, The University of Tokyo, 7-3-1 Hongo, Bunkyo, Tokyo 113-0033, Japan*

[12] *The Caltech Optical Observatories, California Institute of Technology, Pasadena, CA 91125, USA*
[13] *Osservatorio di Astrofisica e Scienza dello Spazio - Istituto Nazionale di Astrofisica, via Gobetti 93/3, I-40129, Bologna, Italy*
[14] *Centro de Astronomía (CITEVA), Universidad de Antofagasta, Avenida Angamos 601, Antofagasta, Chile*
[15] *University of Bologna, Department of Physics and Astronomy (DIFA), Via Gobetti 93/2, I-40129, Bologna, Italy*
[16] *INAF - Osservatorio Astrofisico di Arcetri, Largo E. Fermi 5, I-50125, Firenze, Italy*
[17] *Niels Bohr Institute, University of Copenhagen, Lyngbyvej 2, DK-2100 Copenhagen, Denmark*
[18] *Space Telescope Science Institute, 3700 San Martin Drive, Baltimore, MD 21218, USA*
[19] *Instituto de Física y Astronomía, Universidad de Valparaíso, Avda. Gran Bretaña 1111, Valparaíso, Chile*
[20] *Cavendish Laboratory, University of Cambridge, 19 J. J. Thomson Ave., Cambridge CB3 0HE, UK*
[21] *Kavli Institute for Cosmology, University of Cambridge, Madingley Road, Cambridge CB3 0HA, UK*
[22] *Department of Astronomy, Cornell University, Space Sciences Building, Ithaca, NY 14853, USA*
[23] *Max-Planck-Institut für Astronomie, Königstuhl 17, D-69117, Heidelberg, Germany*
[24] *Leiden Observatory, Leiden University, PO Box 9500, 2300 RA Leiden, The Netherlands*